Quarkonium feed-down and sequential suppression

S. Digal, P. Petreczky, and H. Satz

Fakultät für Physik, Universität Bielefeld, D-33501 Bielefeld, Germany

About 40–50 % of the quarkonium ground states $J/\psi(1S)$ and $\Upsilon(1S)$ produced in hadronic collisions originate from the decay of higher excitations. In a hot medium, these higher states are dissociated at lower temperatures than the more tightly bound ground states, leading to a sequential suppression pattern. Using new finite temperature lattice results, we specify the in-medium potential between heavy quarks and determine the dissociation points of different quarkonium states. On the basis of recent Collider Detector at Fermilab (CDF) data on bottomonium production, we then obtain first predictions for sequential Υ suppression in nuclear collisions.

I. INTRODUCTION

The large values of the charm and bottom quark masses permit potential theory to provide a realistic account of quarkonium spectroscopy [1–3]. From these studies, it is known that the intrinsic length scales of quarkonia are much smaller than those of the usual hadrons, with $r_{J/\psi} \sim 0.2$ fm and $r_\Upsilon \sim 0.1$ fm for the radii of the lowest $c\bar{c}$ and $b\bar{b}$ vector mesons, respectively, in contrast with about 1 fm for light $q\bar{q}$ state radii. This "short-distance" nature of quarkonium states suggests that at least some features of their production in hadronic collisions should be accessible to perturbative QCD calculations, and that indeed turns out to be the case.

The simplest and most general model for quarkonium production, the color evaporation model [4], postulates that the cross section for the production of a given charmonium or bottonium state is simply a fixed (energy-independent) fraction of the corresponding perturbatively calculated $c\bar{c}$ or $b\bar{b}$ production cross section. The resulting predictions for the energy variation of the J/ψ and Υ hadroproduction cross sections are experimentally very well confirmed, for the Υ over a range from $\sqrt{s} \simeq 20$ to 1800 GeV [5]. The assumed energy independence of the production ratios of $2S/1S$ and $3S/1S$ states is found to hold over the same range [5].

Higher quarkonium excitations decay into lower states with generally known branching ratios and widths. As an example, the $\psi' = \psi(2S)$ decays into $J/\psi(1S) +$ anything with a branching ratio of 55%, after a mean lifetime of more than 10^3 fm. As a consequence, J/ψ or Υ production in hadronic collisions occurs in part through the production of higher excited states which subsequently decay into the quarkonium ground states. It is known experimentally that for both J/ψ and Υ about 40–50 % of the hadroproduction rate is due to such feed-down from higher excitations [6–10].

Quarkonium production through feed-down becomes particularly interesting when quarkonium states are used to probe the hot and dense medium created in high energy nuclear collisions. It was predicted that color deconfinement (quark-gluon plasma formation) would lead to J/ψ suppression, since sufficiently hot deconfined media dissolve any $c\bar{c}$ binding [11]. However, different quarkonium excitations will

dissolve at different temperatures of the medium [12], and through a lowering of the open charm (b flavor) threshold with temperature, dissociation by $D\bar{D}$ or $B\bar{B}$ decay becomes possible for higher excited states even below the deconfinement point [13]. Since the lifetime of the excitations is much larger than that of the medium, feed-down production will result in a characteristic sequential suppression pattern [14,15], with the fraction of J/ψ or Υ produced through the decay of higher excitations becoming suppressed at lower temperatures than in the directly produced ground states.

To fully predict this sequential suppression, two prerequisites are needed. We have to know what fractions of the quarkonium ground state production originate from which higher excitations, and we have to know at what temperature or energy density of the hot medium a given excitation dissolves. The first can be determined either experimentally or through a viable model for quarkonium hadroproduction. The second is a well-defined problem for finite temperature lattice QCD studies. At present, neither problem is completely solved. However, in the case of charmonium, the production rates of the higher excitations are experimentally known, and for bottonium production, recent Fermilab data [10,9] provide the basis for fairly reliable estimates. This determines the structure (i.e., the sequence and the different heights) of the various suppression steps for J/ψ and Υ production, but not the actual positions of these steps as function of the temperature or energy density. To estimate these, we make use of recent lattice studies calculating the temperature behavior of the heavy quark potential in full QCD [13,16]. As a result, we obtain a modified J/ψ suppression pattern [14,15], including the decay of ψ' and χ_c in confined matter [13], and then first quantitative predictions for the sequential Υ suppression to be studied in forthcoming BNL Relativistic Heavy Ion Collider (RHIC) and CERN Large Hadron Collider (LHC) experiments.

The structure of this paper is the following. In Sec. II, we first summarize the hadroproduction cross sections for the different charmonium states and then determine the corresponding bottonium cross sections from the mentioned new Collider Detector at Fermilab (CDF) data. As a result, we can fully describe the origin of the J/ψ and Υ produced in hadronic collisions in terms of feed-down from higher ex-

TABLE I. Cross sections for direct charmonium production in $\pi^- N$ and pN collisions, normalized to the overall J/ψ production cross section in the corresponding reaction [8]; feed-down fractions and mass gap to the open charm threshold.

State	$R_i(\pi^- N)$	$R_i(pN)$	$f_i(\pi^- N)$ (%)	$f_i(pN)$ (%)	E_{dis} (MeV)
$J/\psi(1S)$	0.57 ± 0.03	0.62 ± 0.04	57 ± 3	62 ± 4	0.642
$\chi_1(1P)$	0.72 ± 0.18	0.60 ± 0.15	20 ± 5	16 ± 4	0.229
$\chi_2(1P)$	1.04 ± 0.29	0.99 ± 0.29	15 ± 4	14 ± 4	0.183
$\psi(2S)$	0.14 ± 0.04	0.14 ± 0.04	8 ± 2	8 ± 2	0.054
J/ψ	1	1	100	100	

cited states. In Sec. III, we consider the temperature dependence of the heavy quark potential obtained in recent lattice QCD studies. Solving the corresponding Schrödinger equation, we then determine in Sec. IV the dissociation parameters for the different states in a deconfined medium. This leads to quantitative estimates of the sequential J/ψ and Υ suppression patterns.

II. QUARKONIUM PRODUCTION AND FEED-DOWN

A. Charmonium states

It is well known that J/ψ production in hadron-hadron collisions is to a considerable extent due to the production and subsequent decay of higher excited $c\bar{c}$ states [6–8]. We shall here summarize the situation following systematic studies using pion and proton beams at 300 GeV incident energy [8]. In the first two columns of Table I, we list the cross sections σ_i^d obtained for the direct production (excluding feed-down) of the different charmonium states $\psi(1S)$, $\chi(1P)$ and $\psi' = \psi(2S)$ in π^--nucleon and p-nucleon interactions, normalized to the overall measured J/ψ cross section $\sigma_{J/\psi}$, which includes all feed-down contributions. Hence $R_i(\pi^- N) \equiv \sigma_i^d(\pi^- N)/\sigma_{J/\psi}(\pi^- N)$ for the directly produced state i in $\pi^- N$ interactions, and similarly for pN collisions.

Making use of the branching ratios $B[\chi_1(1P) \rightarrow \psi(1S)] = 0.27 \pm 0.02$, $B[\chi_2(1P) \rightarrow \psi(1S)] = 0.14 \pm 0.01$, and $B[\psi(2S) \rightarrow \psi(1S)] = 0.55 \pm 0.05$, one obtains the fractional feed-down contributions f_i of the different charmonium states to the observed J/ψ production; these are shown in the next two columns of Table I. Also listed are the dissociation energies E_{dis}^i,

$$E_{\text{dis}}^i \equiv 2M_D - M_i, \tag{1}$$

measuring how far the mass of state i lies below the zero-temperature open charm threshold $2M_D = 3.740$ GeV.

From Table I it is seen that some 60% of the observed J/ψ are directly produced, about 30% come from χ and about 10% from ψ' decay. According to the color evaporation model, feed-down fractions as well as cross section ratios are energy independent. The results shown in Table I for the ratio of ψ' to overall J/ψ production are in excellent agreement with a variety of experimental results over the range $\sqrt{s} = 18$–65 GeV, which give 0.14 ± 0.034 as average [5]. Even Tevatron results at $\sqrt{s} = 1.8$ TeV for charmonium

transverse momenta $p_T \gtrsim 5$ GeV lead to 0.19 ± 0.05 and are thus within errors in accord with the quoted average value. Similarly, the ratio of χ to J/ψ production is found to be constant over the range $\sqrt{s} = 7$–65 GeV [5]. As noted, the color evaporation model postulates that the different charmonium state cross sections σ_i^d are constant (i.e., energy-independent) fractions c_i of the overall "hidden charm" cross section

$$\sigma_i^d(s) = c_i \sigma_{c\bar{c}}(s) \quad \text{with} \quad M_{c\bar{c}} \lesssim 2M_D. \tag{2}$$

This assumption is thus indeed very well satisfied, even though the corresponding production cross sections themselves vary considerably in the energy range in question, in accord with the perturbatively calculable variation of $\sigma_{c\bar{c}}(s)$. Note that $\Sigma_i c_i \ll 1$, since more than half of the $c\bar{c}$ pairs formed with $M_{c\bar{c}} < 2M_D$ acquire the missing energy from the color field and then contribute to open charm production.

The color evaporation model does not predict the values of the factors c_i. More detailed arguments do, however, lead to some relations between the different cross sections. Projecting a color singlet $c\bar{c}$ state onto different quantum number configurations leads to the estimate [18]

$$\frac{\sigma^d(2S)}{\sigma^d(1S)} \simeq \frac{\Gamma(\psi(2S) \rightarrow e^+ e^-)}{\Gamma(\psi(1S) \rightarrow e^+ e^-)} \left(\frac{M_{J/\psi}}{M_{\psi'}} \right)^3 \simeq 0.24, \tag{3}$$

where Γ denotes the corresponding dilepton decay width of the state in question, and M its mass. The values 0.23 ± 0.06 and 0.22 ± 0.05 obtained from Table I for $\pi^- N$ and pN collisions, respectively, agree well with relation (3).

The ratios between the different $\chi_l(1P)$ states are predicted to be governed essentially by the orbital angular momentum degeneracy [19]; we thus expect for the corresponding cross sections

$$\chi_0(1P):\chi_1(1P):\chi_2(1P) = 1:3:5. \tag{4}$$

From Table I we have for $\pi^- N$ collisions $\chi_2(1P)/\chi_1(1P) \simeq 1.44 \pm 0.38$ and thus reasonable agreement with the predicted ratio 1.67. For pN interactions, the experiment measures only the combined effect of χ_1 and χ_2 decay (30% of the overall J/ψ production); the listed values are obtained by distributing this in the ratio 3:5.
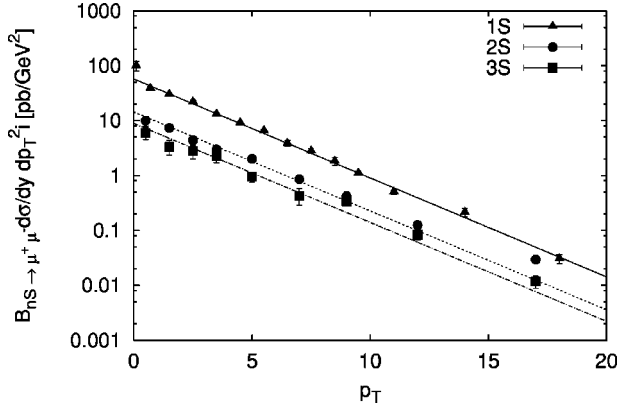
FIG. 1. The transverse momentum dependence of the inclusive production cross sections for different (nS) bottomonium states; the lines are exponential fits.

B. Bottonium states

Production cross sections for the different (nS) bottonium states below the open beauty threshold are known over a considerable energy range [5,9], and as for charmonia, the resulting ratios are with very good precision energy independent [5]. Corresponding cross sections for the sub-threshold (nP) states are so far available only for transverse momenta $p_T \geq 8$ GeV/c [10]. To analyze the complete feed-down pattern, we thus have to find a way to extrapolate these data to $p_T = 0$.

In Fig. 1, we show the p_T distributions of the Υ, Υ', and Υ'' states. It is evident that they exhibit a very similar transverse momentum behavior, which can be parametrized quite well by the form

$$\frac{d\sigma^i}{dy\,dp_T^2} = N_i \exp\{(-0.415)p_T\}, \qquad (5)$$

where N_i specifies the overall cross section values of the different states i. We shall therefore now assume that all bottonium states, nP as well as nS, are governed by the same p_T distribution, so if we know a production ratio in one p_T inteval, we know the ratio of the overall cross sections. To test the validity of assuming such a universal p_T dependence, we have compared data for the different nS states taken in the interval $1 \leq p_T \leq 18$ GeV to an extrapolation of corresponding data for $8 \leq p_T \leq 18$ GeV. The resulting difference of about 10% indicates the uncertainty inherent in our procedure.

To complete the feed-down analysis, we need the decay branching ratios from higher to lower bottonium states, which can be readily computed from the Particle Data Group compilation. From the measured cross sections including feed-down effects (denoted by σ) we now want to reconstruct the direct production cross sections (denoted by σ_i^d) of all sub-threshold bottonium states i. This leads to the relations

$$\sigma(\Upsilon) = \sum_i B[i \to \Upsilon]\sigma_i^d, \qquad (6)$$

TABLE II. Cross sections for direct bottomonium production in $\bar{p}$-p collisions, normalized to the overall Υ production cross section [10,9]; feed-down fractions and mass gap to the open bottom threshold; feed-down fractions obtained in nonrelativistic QCD) (NRQCD).

State	$R_i(\bar{p}p)$	$f_i(\bar{p}p)$ (%)	E_{dis} (GeV)	$f_i(\bar{p}p)_{\mathrm{NRQCD}}$ (%)
$\Upsilon(1S)$	0.52 ± 0.09	52 ± 9	1.098	0.52 ± 34
$\chi_b(1P)$	1.08 ± 0.36	26 ± 7	0.670	0.24 ± 8
$\Upsilon(2S)$	0.33 ± 0.10	10 ± 3	0.535	8 ± 7
$\chi_b(2P)$	0.84 ± 0.4	10 ± 7	0.305	14 ± 4
$\Upsilon(3S)$	0.20 ± 0.04	2 ± 0.5	0.203	2 ± 2
Υ	1	100		100

$$\sigma(\Upsilon') = \sum_i B[i \to \Upsilon']\sigma_i^d, \qquad (7)$$

and

$$\sigma(\Upsilon'') = \sigma^d(3S) \qquad (8)$$

for the three different $b\bar{b}$ S states. The branching ratios $B[i \to \Upsilon]$ and $B[i \to \Upsilon']$ are compiled in [21].

The experiment [10] further provides the fractions F_Υ^{1P} and F_Υ^{2P} of Υ production coming from the different $1P$ and $2P$ χ_b states. For these fractions we know

$$F_\Upsilon^{1P}\sigma(\Upsilon) = \sum_i B[i \to (1P)]B[(1P) \to \Upsilon]\sigma_i^d \qquad (9)$$

and

$$F_\Upsilon^{2P}\sigma(\Upsilon) = \sum_i B[i \to (2P)]B[(2P) \to \Upsilon]\sigma_i^d \qquad (10)$$

in terms of the direct production cross sections for the different states. The branching ratios are again given in [21]. Equations (9) and (10) illustrate that the observed χ_b states that can decay into Υ arise themselves in part through feed-down from still higher excited states. We have to specify the different fractions for this, since e.g. the melting of the $\Upsilon(2S)$ will also remove that fraction of the observed $\chi_b(1S)$ production that comes from $\Upsilon(2S)$ decay.

The experimental values for F_Υ^{1P} and F_Υ^{2P} are given in [10] for transverse momenta $p_T \geq 8$ GeV/c. Since the different S states show a universal p_T dependence, we assume the same to hold for the P states and thus take the measured values

$$F_\Upsilon^{1P} = 0.27 \pm 0.11, \qquad F_\Upsilon^{2P} = 0.11 \pm 0.06 \qquad (11)$$

to remain applicable for the entire p_T range. Making use of the measured overall cross sections $\sigma_\Upsilon = 26.9 \pm 0.6$ mb, $\sigma_{\Upsilon'} = 13.1 \pm 0.5$ mb and $\sigma_{\Upsilon''} = 5.5 \pm 0.5$ mb, we can then solve the five equations (6)–(10) for the different direct production cross sections. The results are shown in Table II, normalized to σ_Υ, together with the relative fractions each state contributes to the overall Υ production. For the P states

χ_b, the shown values are based on the overall cross section $\sigma(\chi_b) = \sigma(\chi_{b0}) + \sigma(\chi_{b1}) + \sigma(\chi_{b2})$, with the three orbital states assumed to contribute in the ratios 1:3:5 [19]. Again we also list the values

$$E_{\text{dis}} = 2M_B - M_i \qquad (12)$$

of the corresponding zero-temperature dissociation energies.

For the feed-down pattern in Υ production we thus find approximately 50% direct $\Upsilon(1S)$ production, 30% from direct $\chi_b(1P)$, 10% from direct $\Upsilon'(2S)$ and 10% from direct $\chi_b(2P)$ production and subsequent decay into $\Upsilon(1S)$. Again the energy independence of these fractions, as required by the color evaporation model, is well satisfied for the measured ratios [5]. To test the consistency of the feed-down pattern with more recent theoretical considerations, we have also calculated the fractions for the whole measured p_T interval using the NRQCD factorization formula [20,21]. The results are presented in the last column of Table II; the details of the calculations are given in the Appendix.

III. THE HEAVY QUARK POTENTIAL IN HOT MEDIA

In finite temperature lattice QCD, the temperature behavior of the static $Q\bar{Q}$ potential $V(T,r)$ is obtained from Polyakov loop correlations measuring the free energy $F(T,r)$,

$$-T \ln\langle L(0)L^+(r)\rangle = F(T,r) + C = V(T,r) - TS + C, \qquad (13)$$

where S denotes the entropy due to the introduction of an unbound $c\bar{c}$ or $b\bar{b}$ pair into the medium and C the (undetermined) Polyakov loop normalization. This can in principle be fixed by requiring that at very short distances, $r \ll T^{-1}$, the potential has the purely Coulombic form α/r, since in the limit $r \to 0$, the effects of the medium should become negligible. At present, however, lattice calculations for high temperatures are probably not yet precise enough to reach the small r range required; for $T \lesssim T_c$, the normalization is found to be more reliable [13]. We therefore here leave C open; as will be seen, this does not affect the determination of the dissociation points of the different bound states; it only prevents a reliable determination of the binding energy. The definition of S in Eq. (13) assumes that for $r \to \infty$, $V(T,r) \to 0 \forall T$. We thus obtain $V(T,r)$ from the relation

$$V(T,r) = -T \ln\left(\frac{\langle L(0)L^+(r)\rangle}{|\langle L\rangle|^2}\right), \qquad (14)$$

where $|\langle L\rangle|^2$ denotes the value of $\langle L(0)L^+(r)\rangle$ for $r \to \infty$.

The free energy (13) was recently studied on $16^3 \times 4$ lattices for 3 and $2+1$ flavor QCD using improved gauge and staggered fermion actions [16,17]. The quark masses used in these studies were $m/T = 0.4$ for 3 flavor and $m_{u,d}/T = 0.4$ and $m_s/T = 1$ for the $2+1$ flavor case. In our analysis we use the 3 flavor potential, for which the analysis is the most complete. However, we have verified that differences between the potentials as functions of rT calculated in the 2 $+1$ and 3 flavor cases are in fact small. The resulting potential in 3 flavor QCD (14) for $T > T_c$ is shown in Fig. 2 for
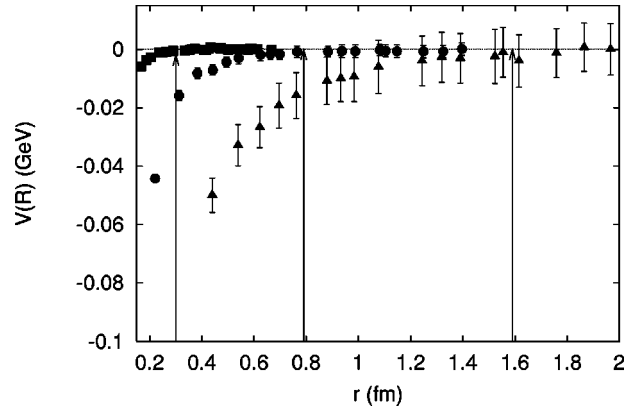

FIG. 2. The color averaged potential at $T = 1.03T_c$ (triangles), $T = 1.45T_c$ (circles) and $T = 3.84T_c$ (squares). The vertical lines indicate the points r_0 beyond which the potential becomes r independent.

some representative temperatures. It is seen that beyond a certain separation distance $r = r_0(T)$, the free energy of the heavy quark system becomes a constant, indicating that within the accuracy of the calculation, the $Q\bar{Q}$ interaction potential vanishes. The resulting $r_0(T)$ as a function of the temperature is given in Fig. 3. Since for $r > r_0(T)$, there is no more interaction between the static color sources, $r_0(T)$ provides a natural limit to all bound state radii.

The potential $V(T,r)$ obtained from Eq. (14) is the average over color singlet and color octet contributions; it can be written in the form

$$V(T,r) = -T \ln\left\{\frac{1}{9}\exp[-V_1(T,r)/T]\right.$$
$$\left. + \frac{8}{9}\exp[-V_8(T,r)/T]\right\}, \qquad (15)$$

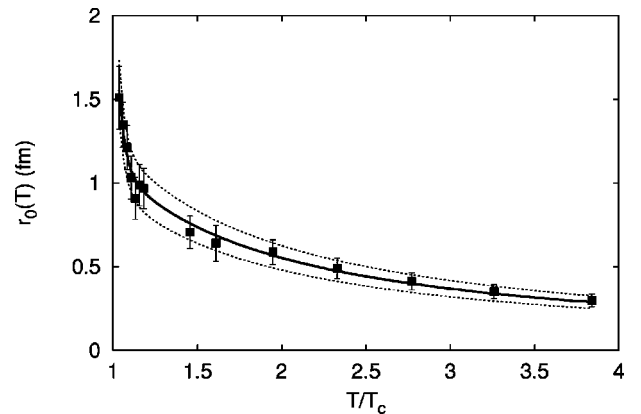where $V_1(T,r)$ and $V_8(T,r)$ specify the singlet and octet

FIG. 3. The temperature dependence of the points r_0 beyond which the potential becomes r-independent. The solid line represents the fit to the data on $r_0(T)$. The dashed lines represent the error band and were estimated by fitting the data on r_0 shifted up (down) by one standard deviation.
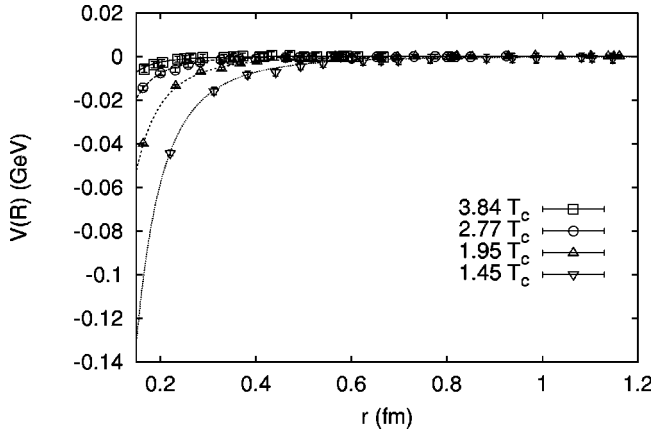
FIG. 4. The color averaged potential for temperatures $T \geqslant 1.45 T_c$; the lines show the fits described in the text.

contributions, respectively. In perturbation theory, the leading terms for both are at high temperature and small r ($r \ll T^{-1}$) of Coulombic form,

$$V_1(T,r) = -\frac{4}{3}\frac{\alpha(T)}{r}, \quad V_8(T,r) = +\frac{1}{6}\frac{\alpha(T)}{r}, \quad (16)$$

with $\alpha(T)$ for the temperature-dependent running coupling. In the region just above the deconfinement point $T = T_c$, there will certainly be significant non-perturbative effects of unknown form. We therefore first consider the high temperature regime, which we somewhat arbitrarily define as $T \geqslant 1.45 T_c$. In this region, we attempt to parametrize the existing non-perturbative effects through a conventional screening form, replacing Eq. (16) by

$$-\frac{3}{4}V_1(T,r) = 6 \ V_8(T,r) = \frac{\alpha(T)}{r}\exp\{-\mu(T)r\}, \quad (17)$$

where $\mu(T)$ denotes the effective screening mass in the deconfined medium.[1] In Fig. 4 we show the fits obtained with the form (15)/(17), assuming $\alpha(T)$ and $\mu(T)$ to be unknown functions of T. The functional form of the potential is seen to be reproduced very well, with the values of $\alpha(T)$ and $\mu(T)$ as given in Figs. 5 and 6. We conclude that in the high temperature regime, a perturbative description modified by color screening gives an excellent account for the lattice results. The screening mass becomes a constant in units of the temperature,

$$\mu(T) = (1.15 \pm 0.02)T. \quad (18)$$

---

[1]The form (17) is actually valid only for $r \gg 1/T$. For the distances $r \leqslant 1/T$ most relevant for quarkonium studies, the screening is determined by the momentum-dependent self-energy $\Pi_{00}(\omega = 0, p)$ [22]. In coordinate space this leads to an r-dependent effective screening mass [23]. In our case this r dependence of the effective screening mass is not important because of the insufficient accuracy of the lattice results, which in 3 flavor QCD can be fitted well with a constant effective screening mass.
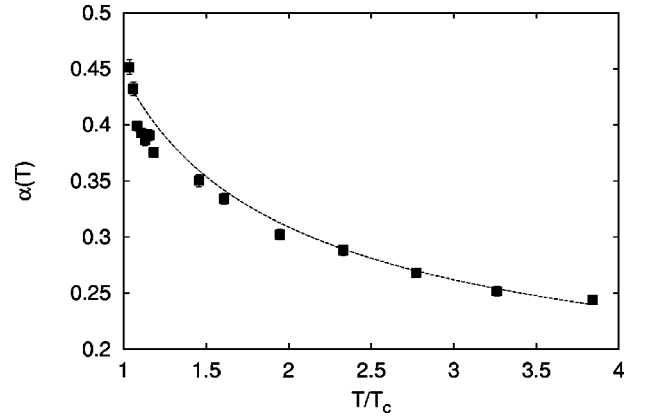

FIG. 5. The temperature dependence of the coupling constant; the line is a fit using the 1-loop running coupling constant formula.

A similar behavior of the screening mass was found in pure SU(2) and SU(3) gauge theory [24–26].

We shall now assume that the form (18) of the screening mass continues to remain valid as we lower the temperature to T_c. Such a constant screening mass down to T_c is again expected from studies of pure gauge theory. There the screening mass determined from the color averaged potential decreases for $T < 1.5 T_c$ as $T \to T_c$ [27]; however, the screening mass determined from the color singlet potential appears to be temperature independent for $T < 10 T_c$ [24–26].

On the other hand, quenched QCD [pure SU(3) gauge theory] studies indicate that when T is lowered to T_c, the perturbative ratio $V_1/V_8 = -8$ will increase in favor of the singlet potential [28]. We therefore try to describe the behavior just above T_c by a potential of the form (15), in which the color octet potential is given by

$$V_8(T,r) = \frac{c(T)}{6}\frac{\alpha(T)}{r}\exp\{-\mu r\} \quad (19)$$

instead of Eq. (17); the factor $c(T) \leqslant 1$ accounts for the expected reduction of octet interactions as $T \to T_c$. In the interval $T_c < T < 1.45 T_c$ we thus fit the lattice results for $V(T,r)$ in terms of the two parameters $c(T)$ and $\alpha(T)$, with $\mu(T)$ given by Eq. (18). In Fig. 7 it is seen that this in fact leads to
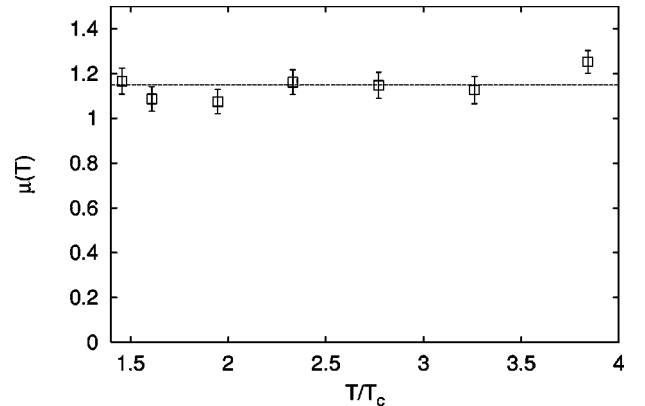

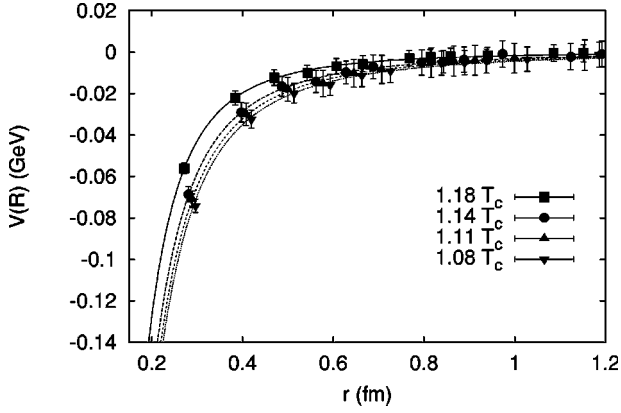FIG. 6. The temperature dependence of the screening mass; the line shows the average value.

FIG. 7. The color averaged potential for low temperatures $T_c < T < 1.45 T_c$; the lines show the fits described in the text.

FIG. 9. The radii (in fm) of J/ψ and Υ states as functions of T/T_c, compared to $r_0(T)$.

an excellent parametrization of the lattice results [16]. The resulting behavior of $c(T)$ is shown in Fig. 8; that of $\alpha(T)$ is included in Fig. 5. From these considerations, we obtain the form (17) for the color singlet potential, in which $\mu(T)$ is given by Eq. (18) and $\alpha(T)$ by Fig. 5.

IV. QUARKONIUM DISSOCIATION IN HOT MEDIA

In the absence of any medium, the masses and radii of the different charmonium and bottonium states are quite well described by non-relativistic potential theory [1–3], based on the Schrödinger equation

$$\left[2m_a + \frac{1}{m_a} \nabla^2 + V_1(r) \right] \Phi_i^a = M_i^a \Phi_i^a, \qquad (20)$$

where $a = c, b$ specifies charm or bottom quarks, i denotes the quarkonium state in question, and r is the separation of the two heavy quarks. Above the deconfinement point, the string tension vanishes and we are left with the singlet potential $V_1(T, r)$ as determined in the previous section. We therefore calculate the bound state radii of the different states, using Eq. (17) in the Schrödinger equation. The radii
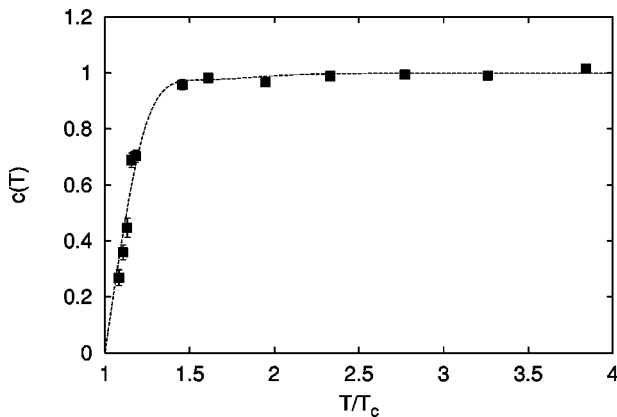

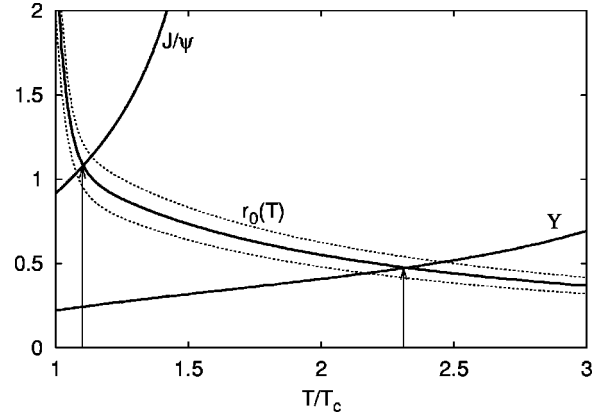FIG. 8. The ratio $-8 V_8 / V_1$ as function of the *temperature*; the line is a fit.

thus obtained then have to be compared to the limiting binding radius $r_0(T)$ in order to specify the dissociation points of the different states.

Before doing this, we have to specify the temperature scale T_c. In the physically interesting case of $2+1$ flavor and physical quark masses it is not very well determined. In the chiral limit of 2 flavor and 3 flavor QCD, one finds $T_c = (173 \pm 16)$ MeV (2 flavor) and $T_c = (154 \pm 16)$ MeV (3 flavor), where the quoted errors are the sum of statistical and estimated systematic discretization errors [16]. For finite u and d quark masses, the critical temperatures coincide in $2+1$ and 2 flavor QCD. We therefore assume that $T_c = 173$ MeV is the relevant critical temperature and use it in our calculations. We have also studied the results obtained with the three-flavor temperature $T = 154$ MeV; the difference turned out to be negligible within the present accuracy of our approach.

In Fig. 9, we illustrate the determination of the dissociation points by comparing the radii of the charmonium and bottonium ground states with the limiting binding radius $r_0(T)$. It is seen that the J/ψ is dissociated at $T \simeq 1.1 T_c$, the Υ at $T \simeq 2.5 T_c$. These results are remarkably consistent with those obtained previously [14] using a screened Cornell potential together with lattice estimates for the screening mass.

We now want to compare the various thresholds for quarkonium dissociation. In Table III, we list the different charmonium states, together with the corresponding dissociation temperatures. For the J/ψ, this is the value $T \simeq 1.1 T_c$ determined above. The χ_c and ψ' radii exceed $r_0(T_c)$, so that these two bound states cannot exist for $T \geq T_c$; the same holds for the $\chi_b(2P)$ and the $\Upsilon(3S)$ states. On the other hand, the dissociation points of the $\chi_b(1P)$ and the $\Upsilon(2S)$ states coincide approximately with that of the J/ψ; all three values are here found to be slightly above T_c. Bearing in mind the unknown systematic errors of the method used here, based on the intersection of $r_0(T)$ and the bound state mass calculated with a screened Coulombic potential, it seems possible only to conclude that these states are dissociated very close to the deconfinement point T_c. This is also consistent with the conclusions reached in the study of the dissociation pattern for $T \to T_c$ from below. The Υ, however, clearly persists up to temperatures well above T_c. In Table

TABLE III. The dissociation parameters of different quarkonium states, as obtained by color screening for $T > T_c$ (present work) and through decay into open charm or b flavor for $T < T_c$ [13].

$q\bar{q}$	T/T_c	$\mu(T_c)/\mu(T)$
J/Ψ	1.10	0.91
$\chi_c(1P)$	0.74	
$\psi(2S)$	0.1–0.2	
$\Upsilon(1S)$	2.31	0.43
$\chi_b(1P)$	1.13	0.88
$\Upsilon(2S)$	1.10	0.91
$\chi_b(2P)$	0.83	
$\Upsilon(3S)$	0.75	

III, we also list the screening masses relative to the deconfinement value $\mu(T_c)$ for those states that survive beyond T_c and are then dissociated by color screening; this provides an indication of the change in the effective screening radius.

Let us next address briefly the survival of those states $(\psi', \chi_c, \Upsilon'', \chi_b')$ that cannot exist for $T \gtrsim T_c$. In earlier studies [12,14], it had been assumed that they are dissociated at $T = T_c$. However, a recent analysis [13], based on the same lattice study as used here [16], shows that they will in fact decay into open charm or beauty states already below T_c. Such a decay becomes possible because the open charm or beauty threshold in a hot confining medium decreases with temperature faster than the masses of the corresponding quarkonium states. The relevant decay temperatures were determined in [13] and are included in Table III.

Using the results of Table III together with the feed-down fractions of Tables I and II, we obtain the suppression patterns shown in Figs. 10 and 11. The new analysis of quarkonia in confined media has thus led to a modified three-step pattern for J/ψ suppression; only the suppression of directly produced J/ψ requires the onset of deconfinement. For the Υ, we obtain the multi-step form shown in Fig. 11. Here again, two states (Υ'', χ_b') decay below T_c; the next two, Υ' and χ_b, are dissociated at or just above T_c, and only the Υ survives much further.

Lattice studies of the kind used here to obtain the heavy quark potential can in principle also determine directly the energy density ϵ of the medium at each temperature, so that
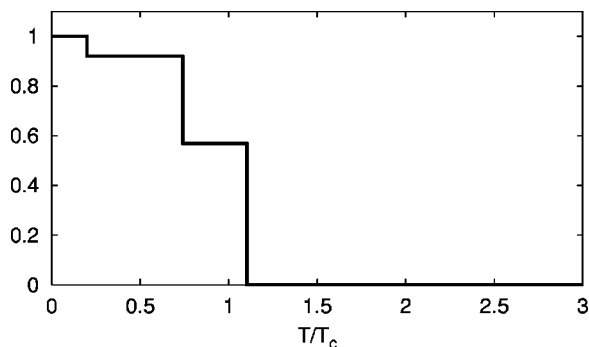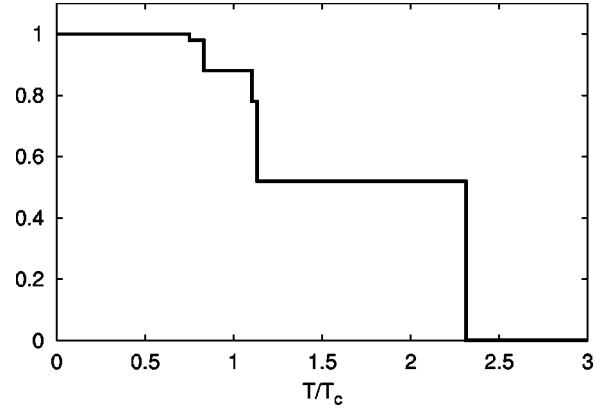

FIG. 10. The J/ψ suppression pattern.

FIG. 11. The Υ suppression pattern.

we should be able to give the dissociation points as well in terms of ϵ. At present, however, various uncertainties (the precision of the T_c determination, the quark mass dependence of T_c and of ϵ, dependence of ϵ on the number of flavors, finite lattice effects) lead to uncertainties of about a factor of 2 in ϵ. A precise determination of this quantity is thus evidently one of the main reasons for insisting on increased computer performance in finite temperature lattice QCD studies; to illustrate, a 10% error in T_c leads to a 50% error in $\epsilon(T_c)$.

V. CONCLUSIONS

In the present work, we have studied quarkonium dissociation by color screening in a deconfining medium. Using new lattice results on the color-averaged potential in full QCD, we have determined the temperature dependence of the color singlet potential. Solving the Schrödinger equation for heavy $Q\bar{Q}$ bound states with the extracted color singlet potential, we have specified the temperatures at which different bound states dissolve. Combining the results of this analysis with those recently found for quarkonium dissociation in a confining medium leads to the suppression patterns summarized in Figs. 10 and 11.

For a more accurate determination of the quarkonium suppression patterns, it would be desirable to carry out direct lattice studies of the color singlet potential and of its quark mass dependence, which may become important near the critical temperature. Furthermore, to make contact with nuclear collision experiments, a more precise determination of the energy density via lattice simulations is clearly needed, as is a clarification of the role of a finite baryochemical potential. For the latter problem, lattice studies are so far very difficult; nevertheless, a recent new approach [29] could make such studies feasible. Finally we note that in hot media the interaction of a quarkonium state with partonic constituents, in particular gluon scattering, can obviously also lead to its dissociation [30,31]. A study of sequential suppression in such a framework would certainly be of considerable interest.

APPENDIX

The NRQCD factorization formula for the inclusive $\Upsilon(nS)$ cross section states is [21]

$$
\begin{aligned}
\sigma[\Upsilon(nS)]_{\mathrm{inc}} = & \; \sigma[b\bar{b}_1(^3S_1)]\langle O_1(^3S_1)\rangle^{\Upsilon(nS)}_{\mathrm{inc}} \\
& + \sum_J \sigma[b\bar{b}_1(^3P_J)]\frac{\langle O_1(^3P_J)\rangle^{\Upsilon(nS)}_{\mathrm{inc}}}{m_b^2} \\
& + \sigma[b\bar{b}_8(^3S_1)]\langle O_8(^3S_1)\rangle^{\Upsilon(nS)}_{\mathrm{inc}} \\
& + \sigma[b\bar{b}_8(^1S_0)]\langle O_8(^1S_0)\rangle^{\Upsilon(nS)}_{\mathrm{inc}} \\
& + \left(\sum_J (2J+1)\sigma[b\bar{b}_8(^3P_J)] \right) \\
& \times \frac{\langle O_8(^3P_0)\rangle^{\Upsilon(nS)}_{\mathrm{inc}}}{m_b^2},
\end{aligned}
\tag{A1}
$$

where $\sigma[b\bar{b}_{1,8}(^{2s+1}L_J)]$ are the short distance cross sections, $\langle O_{1,8}(^{2s+1}L_J)\rangle^{\Upsilon(nS)}_{\mathrm{inc}}$ are the inclusive NRQCD matrix elements, which are non-perturbative [21], and m_b is the mass of the b quark. The indices 1 and 8 refer to color singlet and color octet states, respectively. In the present analysis the short distance cross sections are not calculated in perturbation theory, but extracted from the experimental data on inclusive cross sections $\sigma[\Upsilon(nS)]_{\mathrm{inc}}$ [10], using the information on matrix elements presented in [21,32]. The color octet matrix elements for $J=0$ states, i.e. $\langle O_8(^1S_0)\rangle^{\Upsilon(nS)}_{\mathrm{inc}}$, $\langle O_8(^3P_0)\rangle^{\Upsilon(nS)}_{\mathrm{inc}}$, are compatible with zero within errors [21]. In fact it was shown that a good description of the experimental data on bottomonium production can be obtained by simply setting these matrix elements to zero [32]. Furthermore $\langle O_1(^3P_0)\rangle^{\Upsilon(nS)}_{\mathrm{inc}}$ is very small and we set it to zero in what follows. We also assume that $\sigma[b\bar{b}_1(^3P_2)]/\sigma[b\bar{b}_1(^3P_1)]=8.3$, as predicted by perturbative calculations [33,34]. With these assumptions, the inclusive cross section for S states can be written as

$$
\begin{aligned}
\sigma[\Upsilon(nS)]_{\mathrm{inc}} = & \; \sigma[b\bar{b}_1(^3S_1)]\langle O_1(^3S_1)\rangle^{\Upsilon(nS)}_{\mathrm{inc}} + \sigma[b\bar{b}_8(^3S_1)] \\
& \times \langle O_8(^3S_1)\rangle^{\Upsilon(nS)}_{\mathrm{inc}} + \frac{\sigma_P}{m_b^2}[8.3\langle O_1(^3P_2)\rangle^{\Upsilon(nS)}_{\mathrm{inc}} \\
& + \langle O_1(^3P_1)\rangle^{\Upsilon(nS)}_{\mathrm{inc}}],
\end{aligned}
\tag{A2}
$$

with $\sigma_P=\sigma[b\bar{b}_1(^3P_1)]$. The inclusive color singlet matrix elements are defined as

$$
\langle O_1(^3S_1)\rangle^{\Upsilon(nS)}_{\mathrm{inc}} = \sum_{m\geqslant n} \langle O_1(^3S_1)\rangle^{\Upsilon(nS)} B[\Upsilon(mS)\rightarrow\Upsilon(nS)],
$$

$$
\begin{aligned}
\langle O_1(^3P_J)\rangle^{\Upsilon(nS)}_{\mathrm{inc}} = & \sum_{m\geqslant n} \langle O_1(^3P_J)\rangle^{\chi_{bJ}(mP)} \\
& \times B[\chi_{bJ}(mP)\rightarrow\Upsilon(nS)],
\end{aligned}
\tag{A3}
$$

where $B[H\rightarrow\Upsilon(nS)]$ are the inclusive branching fractions [21], and $\langle O_1(^3S_1)\rangle^{\Upsilon(nS)}$ and $\langle O_1(^3P_J)\rangle^{\chi_{bJ}(mP)}$ are the direct color singlet matrix elements. The latter can be related to the $b\bar{b}$ wave function (or its derivative) at the origin [20]; we have taken this from [3], calculated for the Buchmüller-Tye potential. The inclusive color octet matrix elements $\langle O_8(^3S_1)\rangle^{\Upsilon(nS)}_{\mathrm{inc}}$ were taken from [32]. Given the inclusive matrix and the Tevatron data on $1S$, $2S$, and $3S$ inclusive production cross sections, one can extract the short distance cross sections $\sigma[b\bar{b}_1(^3S_1)]$, $\sigma[b\bar{b}_8(^3S_1)]$ and σ_P. From the short distance cross sections we can estimate the direct cross section for different quarkonium states,

$$
\begin{aligned}
\sigma_d[\Upsilon(nS)] = & \; \sigma[b\bar{b}_1(^3S_1)]\langle O_1(^3S_1)\rangle^{\Upsilon(nS)} \\
& + \sigma[b\bar{b}_8(^3S_1)]\langle O_8(^3S_1)\rangle^{\Upsilon(nS)},
\end{aligned}
$$

$$
\sigma_d[\chi_{bJ}(nP)] = \sigma[b\bar{b}_1(^3P_J)]\langle O_1(^3P_J)\rangle^{\chi_{bJ}(nP)}/m_b^2.
\tag{A4}
$$

In the direct cross section for the χ_{bJ} states we have neglected the color octet contribution which is proportional to $\langle O_8(^3S_1)\rangle^{\chi_{bJ}(nP)}$, in accordance with the results of [32], where it was shown that χ_{bJ} states are predominantly produced by a color singlet mechanism. Also the analysis of Ref. [21] shows that the matrix elements $\langle O_8(^3S_1)\rangle^{\chi_{bJ}(nP)} \simeq 0$. To complete our analysis we have to estimate the direct color octet matrix elements entering in Eq. (A4). With the assumption that $\langle O_8(^3S_1)\rangle^{\chi_{bJ}(nP)}=0$ we can write for the direct color octet matrix elements

$$
\begin{aligned}
\langle O_8(^3S_1)\rangle^{\Upsilon(1S)}_{\mathrm{inc}} = & \langle O_8(^3S_1)\rangle^{\Upsilon(1S)} + B[\Upsilon(2S)\rightarrow\Upsilon(1S)] \\
& \times \langle O_8(^3S_1)\rangle^{\Upsilon(2S)} + B[\Upsilon(3S)\rightarrow\Upsilon(1S)] \\
& \times \langle O_8(^3S_1)\rangle^{\Upsilon(3S)}
\end{aligned}
$$

$$
\begin{aligned}
\langle O_8(^3S_1)\rangle^{\Upsilon(2S)}_{\mathrm{inc}} = & \langle O_8(^3S_1)\rangle^{\Upsilon(2S)} + B[\Upsilon(3S)\rightarrow\Upsilon(2S)] \\
& \times \langle O_8(^3S_1)\rangle^{\Upsilon(3S)}
\end{aligned}
$$

$$
\langle O_8(^3S_1)\rangle^{\Upsilon(3S)}_{\mathrm{inc}} \approx \langle O_8(^3S_1)\rangle^{\Upsilon(3S)}.
\tag{A5}
$$

Finally, multiplying the direct cross section for different bottomonium states by the corresponding inclusive branching fractions from [21], we obtain the feed-down fractions given in Table II.

[1] E. Eichten *et al.*, Phys. Rev. D **17**, 3090 (1978); **21**, 203 (1980).

[2] S. Jacobs *et al.*, Phys. Rev. D **33**, 3338 (1986).

[3] E. Eichten and C. Quigg, Phys. Rev. D **52**, 1726 (1995).

[4] M.B. Einhorn and S.D. Ellis, Phys. Rev. D **12**, 2007 (1975); H. Fritzsch, Phys. Lett. **67B**, 217 (1977); M. Glück, J.F. Owens, and E. Reya, Phys. Rev. D **17**, 2324 (1978); J. Babcock, D. Sivers, and S. Wolfram, *ibid.* **18**, 162 (1978).

[5] R. Gavai *et al.*, Int. J. Mod. Phys. A **10**, 3043 (1995).

[6] J.H. Cobb *et al.*, Phys. Lett. **72B**, 497 (1978); C. Koukoumelis *et al.*, *ibid.* **81B**, 405 (1979).

[7] Y. Lemoigne *et al.*, Phys. Lett. **113B**, 509 (1982).

[8] L. Antoniazzi *et al.*, Phys. Rev. D **46**, 4828 (1992); Phys. Rev. Lett. **70**, 383 (1993).

[9] CDF Collaboration, F. Abe *et al.*, Phys. Rev. Lett. **75**, 4358 (1995).

[10] CDF Collaboration, T. Affolder *et al.*, Phys. Rev. Lett. **84**, 2094 (2000); CDF Note 5027.

[11] T. Matsui and H. Satz, Phys. Lett. B **178**, 416 (1986).

[12] F. Karsch, M.T. Mehr, and H. Satz, Z. Phys. C **37**, 617 (1988).

[13] S. Digal, P. Petreczky, and H. Satz, Phys. Lett. B **514**, 57 (2001).

[14] F. Karsch and H. Satz, Z. Phys. C **51**, 209 (1991).

[15] S. Gupta and H. Satz, Phys. Lett. B **283**, 429 (1992).

[16] F. Karsch, E. Laermann, and A. Peikert, Nucl. Phys. **B605**, 574 (2001).

[17] F. Karsch and E. Laermann (private communication).

[18] See e.g. G. Schuler, hep-ph/9403393.

[19] See e.g. M. Mangano, hep-ph/9507353.

[20] G.T. Bodwin, E. Braaten, and G.P. Lepage, Phys. Rev. D **51**, 1125 (1995).

[21] E. Braaten, S. Fleming, and A.K. Leibovich, Phys. Rev. D **63**, 094006 (2001).

[22] J.C. Gale and J. Kapusta, Phys. Lett. B **198**, 89 (1987).

[23] P. Petreczky *et al.*, hep-lat/0103034.

[24] U.M. Heller, F. Karsch, and J. Rank, Phys. Lett. B **355**, 511 (1995).

[25] U.M. Heller, F. Karsch, and J. Rank, Phys. Rev. D **57**, 1438 (1998).

[26] A. Cucchieri, F. Karsch, and P Petrecsky, Phys. Rev. D **64**, 036001 (2001).

[27] O. Kaczmarek *et al.*, Phys. Rev. D **62**, 034021 (2000).

[28] N. Attig *et al.*, Phys. Lett. B **209**, 65 (1988).

[29] Z. Fodor and S.D. Katz, hep-lat/0104001.

[30] D. Kharzeev and H. Satz, Phys. Lett. B **334**, 155 (1994).

[31] D. Kharzeev *et al.*, Phys. Rev. C **53**, 3051 (1996).

[32] J.L. Domenech-Garret and M.A. Sanchis-Lozano, Nucl. Phys. **B601**, 359 (2001).

[33] R. Baier and R. Rückl, Z. Phys. C **19**, 251 (1983).

[34] R. Gastmans, W. Troost, and T.T. Wu, Nucl. Phys. **B291**, 731 (1987).